Temporal Subtraction of Serial CT Images with Large Deformation Diffeomorphic Metric Mapping in the Identification of Bone Metastases

AUTHOR(S):

Sakamoto, Ryo; Yakami, Masahiro; Fujimoto, Koji; Nakagomi, Keita; Kubo, Takeshi; Emoto, Yutaka; Akasaka, Thai; ... Miller, Michael I.; Mori, Susumu; Togashi, Kaori

CITATION:

Sakamoto, Ryo ...[et al]. Temporal Subtraction of Serial CT Images with Large Deformation Diffeomorphic Metric Mapping in the Identification of Bone Metastases. Radiology 2017, 285(2): 629-639

ISSUE DATE:

2017-11

URL:

http://hdl.handle.net/2433/226817

Temporal Subtraction of Serial CT Images with Large Deformation Diffeomorphic Metric Mapping in the Identification of Bone Metastases[1]

Ryo Sakamoto, MD, PhD
Masahiro Yakami, MD, PhD
Koji Fujimoto, MD, PhD
Keita Nakagomi, MS
Takeshi Kubo, MD, PhD
Yutaka Emoto, MD, PhD
Thai Akasaka, MD
Gakuto Aoyama, MS
Hiroyuki Yamamoto, PhD
Michael I. Miller, PhD
Susumu Mori, PhD
Kaori Togashi, MD, PhD

Purpose: To determine the improvement of radiologist efficiency and performance in the detection of bone metastases at serial follow-up computed tomography (CT) by using a temporal subtraction (TS) technique based on an advanced nonrigid image registration algorithm.

Materials and Methods: This retrospective study was approved by the institutional review board, and informed consent was waived. CT image pairs (previous and current scans of the torso) in 60 patients with cancer (primary lesion location: prostate, $n = 14$; breast, $n = 16$; lung, $n = 20$; liver, $n = 10$) were included. These consisted of 30 positive cases with a total of 65 bone metastases depicted only on current images and confirmed by two radiologists who had access to additional imaging examinations and clinical courses and 30 matched negative control cases (no bone metastases). Previous CT images were semiautomatically registered to current CT images by the algorithm, and TS images were created. Seven radiologists independently interpreted CT image pairs to identify newly developed bone metastases without and with TS images with an interval of at least 30 days. Jackknife free-response receiver operating characteristics (JAFROC) analysis was conducted to assess observer performance. Reading time was recorded, and usefulness was evaluated with subjective scores of 1–5, with 5 being extremely useful and 1 being useless. Significance of these values was tested with the Wilcoxon signed-rank test.

Results: The subtraction images depicted various types of bone metastases (osteolytic, $n = 28$; osteoblastic, $n = 26$; mixed osteolytic and blastic, $n = 11$) as temporal changes. The average reading time was significantly reduced (384.3 vs 286.8 seconds; Wilcoxon signed rank test, $P = .028$). The average figure-of-merit value increased from 0.758 to 0.835; however, this difference was not significant (JAFROC analysis, $P = .092$). The subjective usefulness survey response showed a median score of 5 for use of the technique (range, 3–5).

Conclusion: TS images obtained from serial CT scans using nonrigid registration successfully depicted newly developed bone metastases and showed promise for their efficient detection.

Online supplemental material is available for this article.

[1] From the Department of Diagnostic Imaging and Nuclear Medicine, Graduate School of Medicine, Kyoto University, 54 Kawaharacho, Shogoin, Sakyo-ku, Kyoto 606-8507, Japan (R.S., M.Y., K.F., T.K., T.A., K.T.); Advanced Information & Real-world Technology Development Center 1, Canon, Kyoto, Japan (K.N., G.A., H.Y.); Clinical Research Center for Medical Equipment Development, Kyoto University Hospital, Shogoin, Sakyo-ku, Kyoto, Japan (K.N., G.A., H.Y.); Department of Medical Science, Kyoto College of Medical Science, Oyama-Higashimachi, Sonobe-cho, Nantan, Kyoto, Japan (Y.E.); Department of Biomedical Engineering, Johns Hopkins University, Baltimore, Md (M.I.M.); Center for Imaging Science, Johns Hopkins University, Baltimore, Md (M.I.M.); Russell H. Morgan Department of Radiology and Radiological Science, The Johns Hopkins University School of Medicine, Baltimore, Md (S.M.); and F.M. Kirby Functional Imaging Center, Kennedy Krieger Institute, Johns Hopkins University, Baltimore, Md (S.M.). From the 2014 RSNA Annual Meeting. Received August 16, 2016; revision requested October 4; revision received March 25, 2017; accepted March 27; final version accepted April 19. **Address correspondence to** R.S. (e-mail: *rs-sakamoto@umin.ac.jp*).

Supported by the Ministry of Education, Culture, Sports, Science and Technology, (the Innovative Techno-Hub for Integrated Medical Bio-imaging of the Project for Developing Innovation Systems) and the National Institute of Neurologic Disorders and Stroke (R01NS084957).

Early and accurate detection of bone metastases is one of the most important tasks in diagnostic imaging. If bone metastases are not treated appropriately, they can cause various complications, such as pathologic fractures, as well as neural compression and pain, which could significantly deteriorate a patient's quality of life.

For a long time, technetium 99m bone scintigraphy has been recognized as one of the most effective methods with which to detect bone metastases, and fluorine 18 (^{18}F) fluorodeoxyglucose (FDG) positron emission tomography (PET) has been shown to be useful because of its high sensitivity and specificity (1–4). Recently, ^{18}F fluoride PET has been reported to have superior sensitivity to bone scintigraphy in the detection of bone metastases (5). Recent advancements in magnetic resonance imaging have enabled whole-body imaging of bone metastases with fine image quality (6). However, those examinations are not always performed routinely in patients with cancer.

For a long time, computed tomography (CT) has been used as the primary modality with which to examine local recurrence and distant metastases for clinical follow-up of patients with cancer. Multidetector CT has been shown to have the ability to depict faint lesions characterized by small osteolytic or osteoblastic changes in trabeculae, the bony cortex of bone metastases, or both (7,8). Although the capability of CT is improving continuously, with finer resolution and a better signal-to-noise ratio, the burden on radiologists to detect metastases has been increasing, posing a substantial challenge because of the huge amount of anatomic information. To improve radiologist efficiency and performance in the detection of bone metastases, we hypothesized that a temporal subtraction (TS) technique could enhance the detection of newly developed bone metastases on CT images. The detection of temporal changes is crucial in interpreting diagnostic images, and the benefit of detecting temporal changes with TS has been described in various fields (9–13); however, use of TS to visualize bone metastases on CT images has not been reported. The purpose of our study was to determine the usefulness of a TS technique based on an advanced nonrigid image registration algorithm, termed large deformation diffeomorphic metric mapping (LDDMM), in the detection of bone metastases on serial follow-up CT images.

Advances in Knowledge

- By using temporal subtraction (TS) images, the average reading time to detect bone metastases on CT images decreased significantly, from 384.3 to 286.8 seconds.
- Although significant improvement in lesion detection could not be shown, with subjective scores of 1–5, observers found that the TS images improved their diagnostic confidence from 3 to 4 in the median.

Materials and Methods

Our study was performed with financial support from a Kyoto University and Canon joint research project (the Innovative Techno-Hub for Integrated Medical Bio-imaging of the Project for Developing Innovation Systems) with additional support from Canon, Anatomy Works, and the Ministry of Education, Culture, Sports, Science and Technology of the Japanese government. Authors at Kyoto University (R.S., M.Y., K.F., T.K., Y.E., T.A., K.T.) controled the inclusion of any data and information that might have presented a conflict of interest. This retrospective study was approved by the institutional review boards, and informed consent was waived.

Subject Population

Images of two serial torso CT studies (previous and current studies) in 60 patients with cancer between 2007 and 2013 were selected sequentially from our clinical database. The study group consisted of 30 patients with positive findings, with newly developed bone metastases only in the current study, and 30 control patients with negative findings without any bone metastases. Inclusion criteria were as follows: *(a)* known site of malignancy, *(b)* CT images obtained at at least two time points were available, and *(c)* one or more subsequent bone scintigraphy or FDG PET/CT study was available. Additional inclusion criteria for positive cases were as follows: *(a)* there were fewer than 10 lesions per patient, *(b)* the minimum lesion diameter was greater than 5 mm, and *(c)* lesions were suggestive of metastases on at least one study (osteolytic and/

Implication for Patient Care

- For follow-up of patients with cancer, this temporal subtraction technique can potentially facilitate more efficient detection of bone metastases at serial CT; however, technical complexity and lack of wide availability remain challenges to the immediate applicability of this technique in the routine clinical care of patients.

https://doi.org/10.1148/radiol.2017161942

Content codes: MK OI

Radiology 2017; 285:629–639

Abbreviations:
FDG = fluorodeoxyglucose
FOM = figure of merit
JAFROC = jackknife free-response receiver operating characteristic
LDDMM = large deformation diffeomorphic metric mapping
TS = temporal subtraction

Author contributions:
Guarantors of integrity of entire study, R.S., M.Y.; study concepts/study design or data acquisition or data analysis/interpretation, all authors; manuscript drafting or manuscript revision for important intellectual content, all authors; approval of final version of submitted manuscript, all authors; agrees to ensure any questions related to the work are appropriately resolved, all authors; literature research, R.S., M.Y., T.K., Y.E., S.M.; clinical studies, R.S., M.Y., K.N., T.K., T.A., G.A., K.T.; experimental studies, R.S., M.Y., K.F., K.N., Y.E., G.A., M.I.M., S.M.; statistical analysis, R.S., M.Y., K.N., G.A., S.M.; and manuscript editing, R.S., M.Y., K.F., K.N., T.K., Y.E., T.A., H.Y., M.I.M., S.M.

Conflicts of interest are listed at the end of this article.

Table 1

Characteristics of the Subjects for the Observer Study

Bone Metastasis	Age (y)*	Sex		Primary Lesion					Average Interval of Scans (mo)*	Scan Coverage			Scan Condition from Previous to Current		
		Male	Female	Breast	Lung	Liver	Prostate			Chest to Pelvis	Chest to Upper Abdomen	Chest	CE to CE	nCE to CE or CE to nCE	nCE to nCE
Negative	66.0 ± 10.6 (45–84)	16	14	8	10	4	8		14.5 ± 8.8 (2–42)	16	5	9	10	3	17
Positive	67.1 ± 8.9 (49–83)	16	14	8	10	6	6		16.0 ± 11.1 (2–41)	15	7	8	13	12	5
Total	66.5 ± 10.6 (45–84)	32	28	16	20	10	14		15.2 ± 9.9 (2–42)	31	12	17	23	15	22

Note.—CE = contrast enhanced, nCE = unenhanced.

* Data are mean ± standard deviation. Data in parentheses are the range.

or osteoblastic change at CT and/or substantial focal uptake at FDG PET or bone scintigraphy). The diagnosis was confirmed by finding continued growth on subsequent CT images or by clinical data supporting the diagnosis of bone metastases. Control subjects and their CT studies were selected to match the age, sex, primary lesion, and scanning interval of the patients with positive findings. These conditions were confirmed, in consensus, by two radiologists (R.S., K.F.: 9 and 13 years of experience in interpretation of torso CT images, respectively) who did not participate in the observer study by consulting all available clinical information registered before and after the current study, including medical records, laboratory data, images, and CT, bone scintigraphy, and FDG PET reports. A total of 65 bone metastases were identified in 30 patients and were considered the reference standard. Imaging area and use of intravenous contrast material varied according to the patient's disease or status. Details of the cases and scanning conditions, the range, and the average interval for paired CT scans are summarized in Table 1.

TS Method

Details of the process for creating TS images are described in Appendix E1 (online) and Figure 1. In brief, previous CT images were manually registered to current ones to match the position of the bronchial bifurcation. The rest was performed automatically; affine transformation was followed by the nonrigid registration algorithm, LDDMM. TS images were obtained by subtracting transformed previous images from current images.

Image Review

The location (humeral head to clavicle, sternum area, scapula, rib, thoracic spine, lumbar spine, pelvis to femoral head area) and the severity of subtraction artifacts on TS images were recorded for each location to evaluate registration quality. Artifacts were graded by using a three-point scale: a score of 1 indicated no artifact; a score of 2, mild to moderate artifact (partial bandlike subtraction artifact in a bone); and a score of 3, severe artifact (bandlike subtraction artifact in a bone and/or apparent misalignment of a bone). The appearances of bone metastases (osteolytic, osteoblastic, or mixed) on TS images were recorded. This image review was performed by two radiologists (R.S., K.F.).

Figure 1

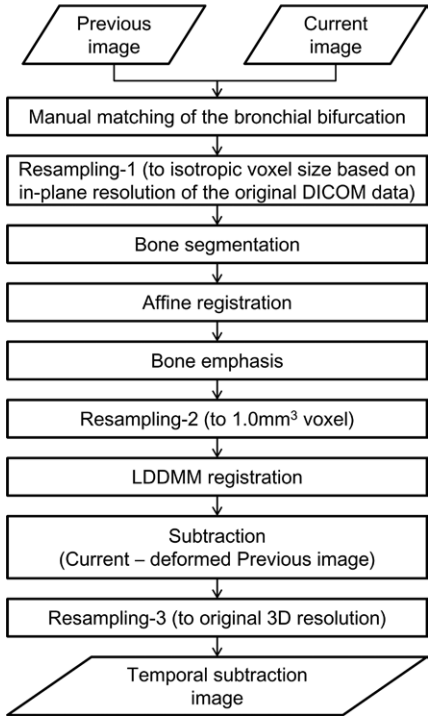

Figure 1: Flowchart of our TS method for skeletal bones. *DICOM* = Digital Imaging and Communications in Medicine, *3D* = three-dimensional.

Observer Study

Seven radiologists (M.Y., T.K., Y.E., T.A.) with 6–28 years of experience in interpretation of torso CT images independently interpreted a pair of current and previous CT images for each subject in the axial stack mode. They were allowed to change the window level and window width. They were asked to identify new bone metastases by marking the location of each suspicious lesion with the percentage likelihood of it being a metastasis. This experiment was a fully crossed multireader multicase

Figure 2

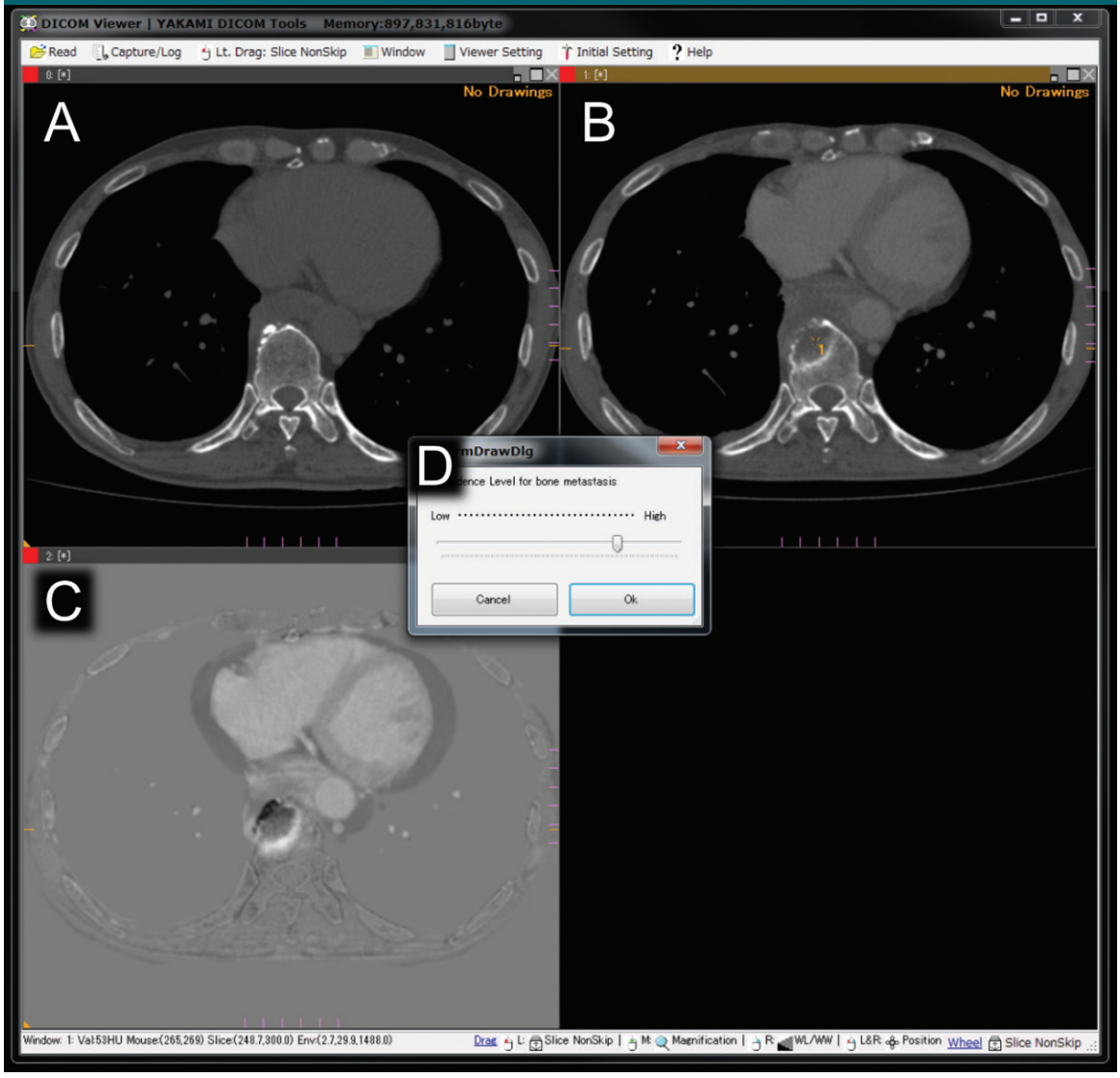

Figure 2: Screenshots of the image viewer for the observer study. The image stacks in the upper row show, *A,* previous and, *B,* current CT images in a 67-year-old man with lung cancer. *C,* TS image. *D,* When an observer clicks on a suspicious lesion, the dialog box for rating the likelihood (low to high) of bone metastasis appears.

study, and it was performed by using an in-house Digital Imaging and Communications in Medicine viewer (Yakami DICOM Tools, version 1.4.5.0; *http://www.kuhp.kyoto-u.ac.jp/~diag_rad/intro/tech/dicom_tools.html*) (Fig 2). Image interpretation was conducted twice for the same cases, first without and then with TS images. The order of cases in each reading session was randomized. An interval of at least 30 days was set between the two reading sessions to minimize the memory effect. To control practice effects, observers were trained to use the viewer with six training cases before an actual observer study. Observers were informed of the patient's age and sex and of histologic findings in the primary tumor and were blinded to all other clinical data. They were asked to rate the confidence level of their interpretation for the entire study (survey 1: 1, very low; 2, low; 3, moderate; 4, high; 5, very high) and of the usefulness of TS images (survey 2: 1, useless; 2, not very useful; 3, somewhat useful; 4, very useful; 5, extremely useful) by using a five-point scale for each case. Reading time to identify new bone metastases was also recorded. After all data were collected, those lesions affected beneficially or detrimentally by TS images were analyzed in terms of lesion location and appearance. TS images were considered beneficial to lesions that at least one radiologist could

detect only with TS images: specifically, lesions that were false-negative without TS images and true-positive with TS images under the condition that a likelihood of 51% or higher was considered positive. Conversely, TS images were considered detrimental to lesions that at least one radiologist could detect only without TS images: specifically, lesions that were true-positive without TS images and false-negative with TS images under the condition. Changes in sensitivity between the sessions without and those with TS images were also analyzed for each location and each appearance of bone metastases.

Statistical Analyses

The difference in age between female and male subjects was analyzed with the Mann-Whitney *U* test. Median scores for subtraction artifacts were compared among areas by using the Kruskal-Wallis test followed by post hoc analysis with the Mann-Whitney *U* test with Bonferroni correction. Interobserver agreement was assessed with weighted κ statistics. Sensitivity of lesion-based analysis, number of false-positive findings per patient, sensitivity and specificity of case-based analysis, reading time, and confidence level were compared between the two sessions by using the Wilcoxon signed rank test. Sensitivity and specificity were analyzed under the condition that a lesion with 51% or higher likelihood of being metastasis was considered a positive finding. For a case-based analysis, a case with at least one positive lesion was considered positive. Jackknife free-response receiver operating characteristic (JAFROC) analysis (14,15) was used to evaluate radiologist performance. The analysis was conducted by using freely available JAFROC software (JAFROC, version 4; *http://www.devchakraborty.com*) with random readers and random cases models. The change in sensitivity was compared among lesion location and appearance by using the Kruskal-Wallis test. SPSS (IBM SPSS Statistics for Windows, version 21.0; IBM, Armonk, NY) was used for statistical analyses, and $P < .05$ indicated a significant difference.

Table 2

Median Score of Subtraction Artifact in Each Location

Statistic	Humeral Head to Clavicle	Sternum	Scapula	Rib	Thoracic Spine	Lumbar Spine	Pelvis to Femoral Head
Median score	2*	1	3*	2*	1	1	1
κ value	0.92	1.00	0.88	0.59	1.00	0.78	0.89

Note.—The subtraction artifact was graded with a three-point scale: 1, no artifact; 2, mild to moderate artifact (partial bandlike subtraction artifact in a bone); and 3, severe (bandlike subtraction artifact in a bone or apparent misalignment of a bone).

* Significantly high compared with the spine and pelvic areas at post hoc analysis ($P < .001$).

Results

The processing time for LDDMM for each case ranged from approximately 2 to 10 hours depending on the scanning area. The average processing time for images of the chest, chest-to-upper abdomen, and chest-to-pelvis were 2 hours 32 minutes, 4 hours 37 minutes, and 6 hours 11 minutes, respectively. The overall mean age was 66.5 years ± 9.6 [standard deviation], and the overall age range was 45–84 years. There were 32 men (mean age, 69.6 years ± 8.6; age range, 52–84 years) and 28 women (mean age, 63.0 years ± 9.5, age range, 45–81 years) ($P = .019$) in this study. The details of the 65 bone metastases considered with the reference standard were as follows: mean size, 20.5 mm ± 14.0; number of bone metastases per patient with positive findings, 2.2 ± 1.3; 28 osteolytic metastases; 26 osteoblastic metastases; and 11 mixed osteolytic and osteoblastic metastases.

The skeletal structure of previous and current CT images was almost perfectly registered except for the humeral head–to-clavicle area, scapulae, and ribs (Table 2). Obvious misalignments were observed more frequently in the scapulae than in other bones. In regard to the subtraction artifacts of ribs, almost all artifacts were noticed at the tips of the ribs. In the cases with positive bone metastasis findings, bone metastases were located in the humeral head and clavicle area ($n = 1$), sternum ($n = 6$), scapulae ($n = 4$), ribs ($n = 13$), thoracic spine ($n = 8$), lumbar spine ($n = 17$), and pelvis-to–femoral head area ($n = 16$). The appearance of bone metastases on TS images varied, depending on the type of lesion. Osteolytic metastases appeared as areas of low signal intensity on TS images (Fig 3a). Osteoblastic changes appeared as areas of high signal intensity (Fig 3b). Mixed osteolytic and osteoblastic metastases had a heterogeneous appearance, with areas of low and high signal intensity (Fig 3c). In some cases, nonneoplastic temporal bone changes, such as degenerative compression fracture, development of Schmorl nodes, healed rib fractures, subchondral cysts, and osteophytes, also were observed. Outside of the skeletal structure, artifacts were observed due to the difference in imaging conditions (eg, with or without contrast material) or large morphologic changes in the gastrointestinal organs. Representative cases with these changes or subtraction artifacts are shown in Figure 4.

The average sensitivity at lesion-based analysis was not significantly increased from 58.0% (37.7 of 65.0) to 65.9% (42.9 of 65.0) when using TS images. The average number of false-positive findings per case was not significantly increased from 0.19 to 0.23 ($P = .344$). The average sensitivity and specificity at case-based analysis were not significantly increased (from 78.0% [23.4 of 30.0] and 92.9% [27.9 of 30.0], respectively, to 80.0% [24.0 of 30.0] and 96.7% [29.0 of 30.0], respectively; $P = .443$ and $P = .066$, respectively). The free-response receiver operating characteristic is shown in Figure 5. The figure of merit (FOM) value (equivalent value of the area under the receiver operating characteristic curve) for each radiologist was improved for

Figure 3

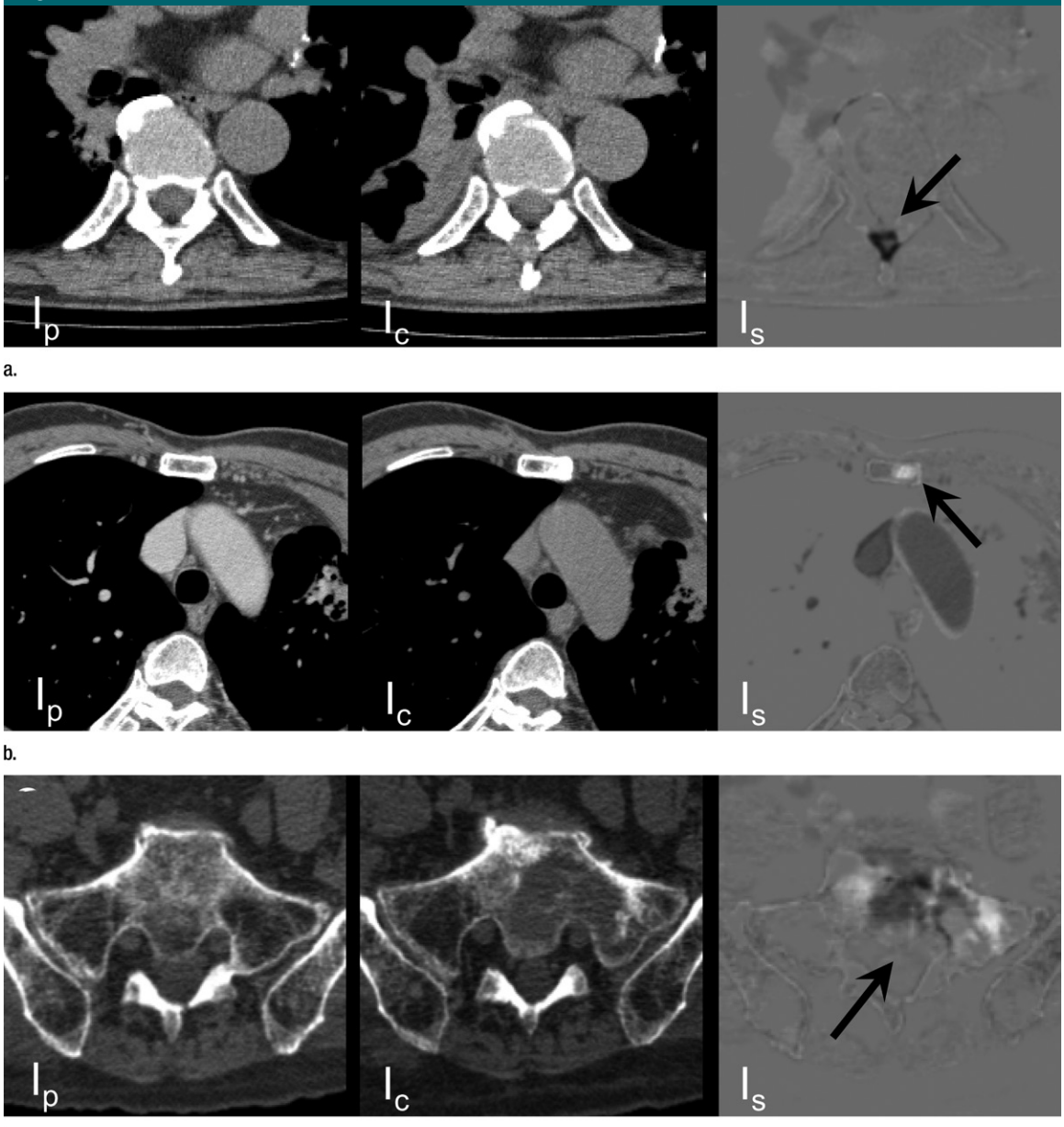

Figure 3: TS images show bone metastases (arrow) with various appearances and locations (I_c, current CT images; I_p, previous CT images; I_s, TS images). **(a)** Osteolytic lesion in a 71-year-old man with lung cancer is hypointense. **(b)** Osteoblastic lesion in a 61-year-old man with lung cancer is hyperintense. **(c)** Mixed osteolytic and osteoblastic lesion in a 66-year-old woman with lung cancer shows heterogeneous intensity.

all observers except one, and the average FOM value was improved from 0.758 to 0.835; however, this difference was not significant (P = .092).

The average reading time was decreased significantly from 384.3 seconds to 286.8 seconds (P = .028). Radiologists' median confidence in their interpretation (survey 1) improved significantly from 3 to 4 (P = .043) when using TS images. Usefulness of TS images (survey 2) yielded sufficiently high scores (median, 5), and all observers recognized the advantage of TS images (3 at minimum). The FOM, reading time, and results of the two surveys are shown in Table 3.

The review of the results showed both beneficial and detrimental effects of TS images (Fig 6). Beneficial effects were seen in 39 lesions; one lesion was beneficially affected for six radiologists, and six lesions were beneficially affected for four radiologists. In these cases, bone metastases appeared as

Figure 4

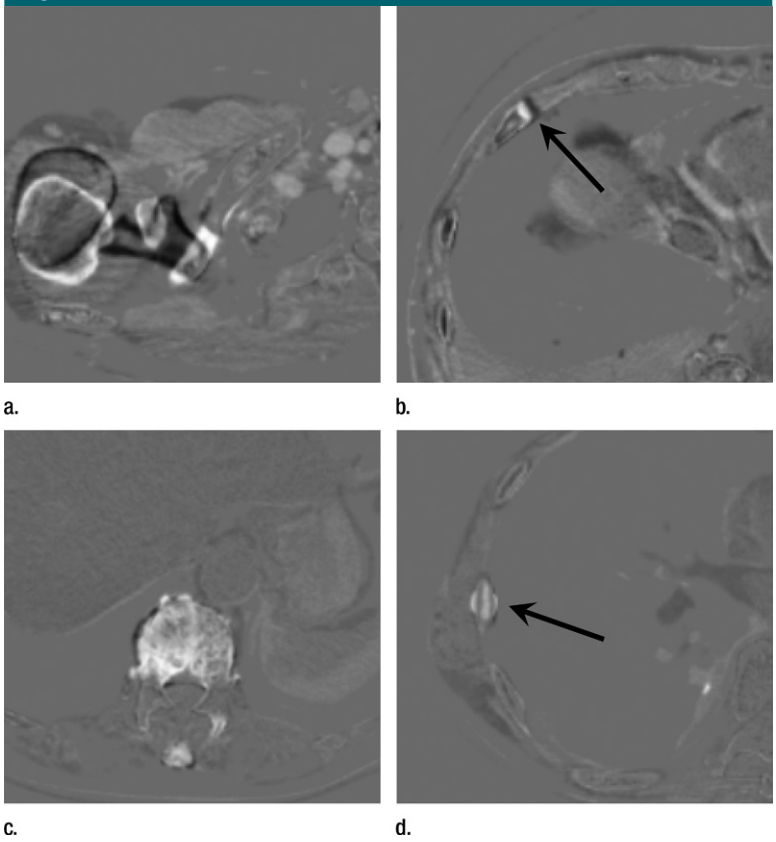

Figure 4: Subtraction artifacts and benign changes on TS images. **(a)** Image in a 64-year-old woman with breast cancer. Obvious misalignments are frequently observed at the humeral head, scapula, or both. Artifacts due to the differences in imaging conditions (subtraction of unenhanced images from contrast-enhanced images) are also observed. **(b)** Image in a 66-year-old woman with breast cancer. The tips of the ribs often show bandlike mild subtraction artifacts (arrow). **(c)** Image in a 76-year-old woman with lung cancer shows a degenerative compression fracture in the thoracic spine. **(d)** Image in a 71-year-old man with lung cancer shows traumatic sclerotic change in a rib (arrow).

small osteolytic lesions, without apparent destruction of the bony cortex. These lesions were found at the ribs, pelvic bones, and posterior column of the vertebrae. Detrimental effects were seen in 33 lesions; four lesions were detrimentally affected for three radiologists, and no lesion was detrimentally affected for more than three radiologists. Three of the four lesions were located on or close to the scapulae, where severe subtraction artifacts were often observed. Both beneficial and detrimental effects were seen in 20 lesions. Examples of these cases, showing the advantages and disadvantages of TS images, are shown in Figure 6.

The appearance- and lesion-wise comparisons of the change in sensitivity showed no significant differences; however, there was a decrease in sensitivity at the scapulae with TS images in this analysis (Table 4).

Discussion

Image registration methods are particularly important in radiation therapy and volumetric imaging (16–18). One of the major applications is TS; however, to our knowledge, this technique has not been put into practical use for clinical CT images, even for the skeletal structure, although it consists of rigid bones. This could be attributed to the substantial differences in bone configurations between serial CT scans due to different patient positioning or degree of inspiration, requiring highly elastic and accurate image transformation for registration. To reduce the misregistration artifacts and enhance the diagnostic value of TS, accurate image registration is inevitable. LDDMM is a well-known nonrigid registration algorithm that is designed to cope with a large amount of deformation. It has been previously confirmed that LDDMM is feasible for serial chest CT images (19). Thus, this method was adopted to create precise TS images in our study. The result showed sufficient registration for skeletal structures on serial CT images to depict the various appearances of bone metastases successfully. Although its incremental value was not significant, our technique showed promise for improving radiologist performance in the detection of bone metastases. It was also shown that improvement did not depend on lesion appearance. Previous TS studies reported that TS is more beneficial for residents who have less experience in diagnostic imaging than attending radiologists (10,11). Since all observers in our study were highly trained radiologists, an investigation with residents remains as a future work. In addition, under the present experimental conditions, the observers were given unlimited time to detect bone metastases. Consequently, they tended to take longer to read CT images when compared with the time spent for their routine clinical work. Thus, investigating the advantage of TS images in the actual clinical setting in a prospective study is also important.

In our study, TS images helped us detect small lytic lesions located at the ribs or pelvic bones. Several computer-aided detection methods for bone metastases at torso CT have been reported previously (20–22); however, they focused only on vertebral lesions. Although vertebrae are the most vulnerable sites for bone metastases (23), metastases can occur at any site in the

Figure 5

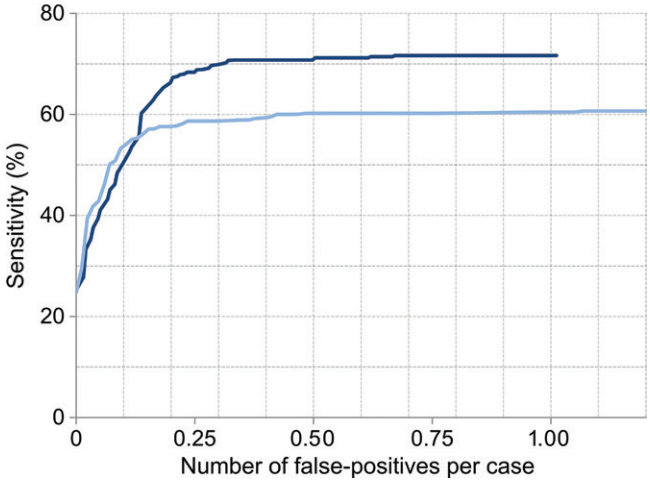

Figure 5: Average free-response receiver operating characteristic curves without (light blue) and with (dark blue) TS images. Radiologist performance increases with TS images, but this difference is not significant ($P = .092$).

Table 3

FOM Values, Reading Times, and Results of Surveys for Seven Radiologists

	FOM		Average Reading Time (sec)		Survey 1*		
Reader	Without TS	With TS	Without TS	With TS	Without TS	With TS	Survey 2*
1	0.863	0.880	494	354	3	4	5
2	0.745	0.860	237	191	3	3	4
3	0.746	0.800	395	343	4	4	5
4	0.761	0.755	151	108	3	4	4
5	0.618	0.890	308	346	3	3	3
6	0.755	0.837	659	424	3	4	5
7	0.818	0.819	446	241	3	4	5
Overall	0.758	0.835	384	287†	3	4	5

Note.—In survey 1, observers were asked to indicate their confidence level for the diagnosis (1, very low; 2, low; 3, moderate; 4, high; 5, very high). In survey 2, observers were asked if the temporal subtraction image was useful (1, useless; 2, not very useful; 3, somewhat useful; 4, very useful; 5, extremely useful).

* Data are medians.

† Shows significant difference.

skeletal bones. Our TS method enabled visualization of bone metastases in all scanned areas, which is highly advantageous when compared with these other methods. In some cases, we used image sets of previous and current CT studies with different conditions of contrast enhancement, since scanning conditions with serial CT are not always the same in the clinical setting. The difference may harm the registration accuracy of bones and may cause subtraction artifacts in enhanced organs or vessels. These issues require further verification. However, the harm would be minute to none due to the higher density of bones versus that of organs, even if enhanced. The artifacts would not substantially hinder radiologists' ability to detect bone metastases because the artifacts are distributed outside of the bones on which radiologists focus their attention during detection. Our method was not sufficiently successful in depicting bone metastases located on or close to the scapulae (change in sensitivity, −0.18) because of subtraction artifacts since the position of the scapulae can vary largely for each scan. Thus, further improvement of registration accuracy for such problematic regions is an important future research target.

When radiologists use a computer-aided diagnosis system, viewing and assessing its output may require additional time (19). However, our TS technique even improved the efficiency of this task in detecting newly developed bone metastasis by significantly decreasing reading time by 25% for this task. The result of the survey also showed increased diagnostic confidence. These results could be understood because less confidence in the diagnosis would lead to repetitive image viewing time.

Our TS images showed not only temporal changes caused by bone metastases but also various nonneoplastic changes, such as degenerative and traumatic changes. Although this seems to confuse radiologists, the result showed sufficiently high average specificity in the detection of metastases. This might be because TS is based on a simple principle, in contrast with computer-aided diagnosis, which typically uses complex image features.

There were several limitations in our study. First, bone lesions were not confirmed at histologic analysis. In the clinical setting, it is rare to perform biopsy to obtain histologic confirmation of bone metastases when a primary lesion is evident. Thus, the best effort was made by consulting all available clinical information, as mentioned in the Subject Population section. Second, this method requires large computational resources and long calculation times because of the large size of thin-section CT image data, and no comparison was made to any other registration algorithm on the aspect of computational effort and registration accuracy. Optimization of the registration algorithm or consideration of a more efficient algorithm will be the subjects of important future work before this system is introduced into the clinical workflow. Third, the LDDMM algorithm was applied solely

Figure 6

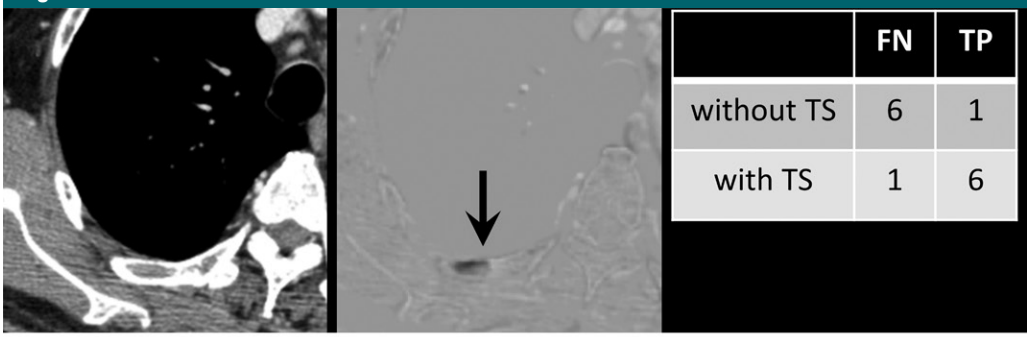

	FN	TP
without TS	6	1
with TS	1	6

a.

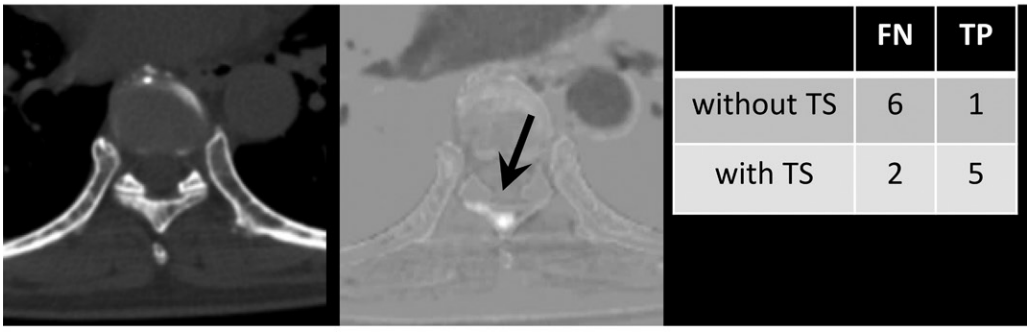

	FN	TP
without TS	6	1
with TS	2	5

b.

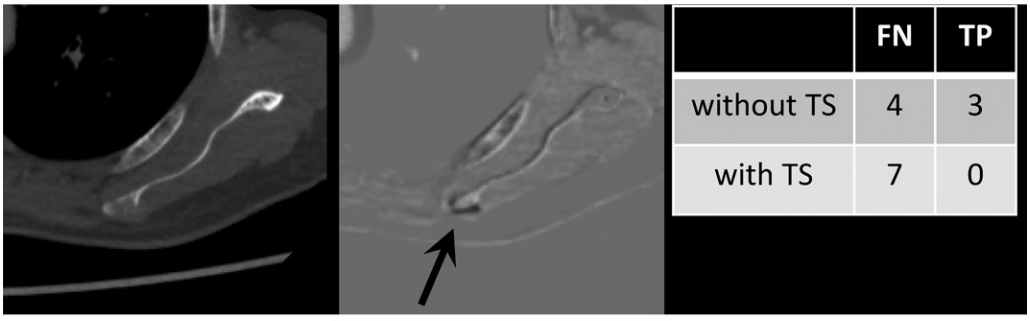

	FN	TP
without TS	4	3
with TS	7	0

c.

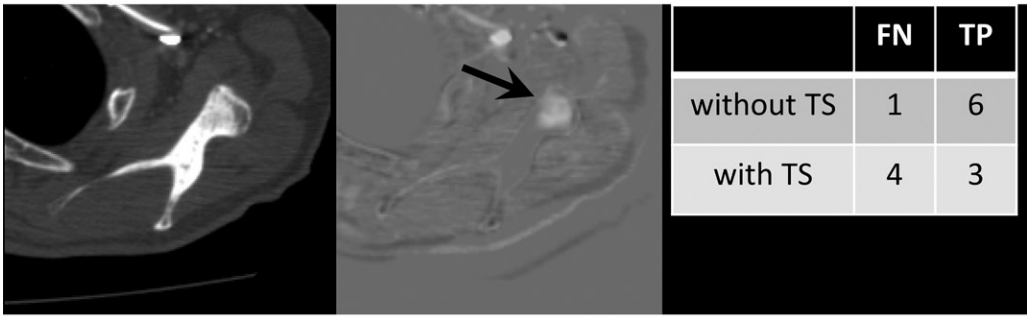

	FN	TP
without TS	1	6
with TS	4	3

d.

Figure 6: Bone metastases that can be detected with TS images and those that cannot. Left column shows current CT images; middle column, TS images; and right column, tables with numbers of radiologists. *FN* = false-negative, *TP* = true-positive. **(a, b)** TS images are especially beneficial in the detection of small osteolytic lesions or metastases, with no apparent destruction of the cortex (**a**, 82-year-old man with hepatocellular carcinoma; **b**, 69-year-old man with prostate cancer). **(c, d)** Bone metastases located on the scapulae are less easily detected on TS images (**c**, 64-year-old woman with breast cancer; **d**, 66-year-old woman with breast cancer).

Table 4

Appearance- and Lesion-wise Comparisons of Change in Sensitivity for Detecting Bone Metastases

	Appearance			Location						
Statistic	Osteolytic ($n = 28$)	Osteoblastic ($n = 26$)	Mixed ($n = 11$)	Humeral Head to Clavicle ($n = 1$)	Sternum ($n = 6$)	Scapula ($n = 4$)	Rib ($n = 13$)	Thoracic Spine ($n = 8$)	Lumbar Spine ($n = 17$)	Pelvis to Femoral Head ($n = 16$)
Average change in sensitivity	0.10	0.07	0.01	0.57	0.00	−0.18	0.12	0.14	0.07	0.05

Note.—A positive observation was defined as a likelihood score of 51% or higher assigned by an observer.

to serial clinical CT scans, without simulations with phantoms. The empirical setting we previously used showed satisfactory results; however, more detailed optimization based on numeric simulations may lead to more precise registration, and this would be one of the future tasks. Fourth, we have not investigated the effect of variability in imaging conditions, such as use of contrast agent and selection of scanning protocol, on TS images of bones. Fifth, we evaluated the utility of TS images only in the detection of newly developed bone metastases. In a previous study, we used a Jacobian map, which indicates local volume change, to visualize temporal changes in existing lesions (19). It could be that a Jacobian map of bone metastasis could reflect temporal changes in the volume or shape of existing lesions. Sixth, since our ultimate goal is to apply this TS technique to patients with cancer with various disease stages, including those who have bone metastases in the initial assessment, our study population may differ from the cancer population (selection bias). Seventh, all observers read the studies without and then with TS images. We consider that the reading-order bias could be kept minimal by setting a reading interval for a washout period; however, the reading order bias might not be completely eliminated.

In conclusion, TS images obtained with serial CT scans and use of nonrigid registration successfully depicted newly developed bone metastases and showed promise for use in their efficient detection.

Disclosures of Conflicts of Interest: R.S. disclosed no relevant relationships. **M.Y.** Activities related to the present article: disclosed no relevant relationships. Activities not related to the present article: is a consultant for Kyoto ProMed; prepared manuscripts for Innervision and Medical Eye. Other relationships: disclosed no relevant relationships. **K.F.** disclosed no relevant relationships. **K.N.** Activities related to the present article: disclosed no relevant relationships. Activities not related to the present article: is a Canon employee. Other relationships: disclosed no relevant relationships. **T.K.** disclosed no relevant relationships. **Y.E.** disclosed no relevant relationships. **T.A.** disclosed no relevant relationships. **G.A.** Activities related to the present article: disclosed no relevant relationships. Activities not related to the present article: is a Canon employee. Other relationships: disclosed no relevant relationships. **H.Y.** Activities related to the present article: disclosed no relevant relationships. Activities not related to the present article: is a Canon employee. Other relationships: disclosed no relevant relationships. **M.I.M.** Activities related to the present article: disclosed no relevant relationships. Activities not related to the present article: is a cofounder of AnatomyWorks; holds U.S. patents 8,594,401 and 8,600,131. Other relationships: disclosed no relevant relationships. **S.M.** Activities related to the present article: disclosed no relevant relationships. Activities not related to the present article: is a cofounder of AnatomyWorks; holds U.S. patents 8,594,401 and 8,600,131. Other relationships: disclosed no relevant relationships. **K.T.** disclosed no relevant relationships.

References

1. Bury T, Barreto A, Daenen F, Barthelemy N, Ghaye B, Rigo P. Fluorine-18 deoxyglucose positron emission tomography for the detection of bone metastases in patients with non-small cell lung cancer. Eur J Nucl Med 1998;25(9):1244–1247.
2. Hahn S, Heusner T, Kümmel S, et al. Comparison of FDG-PET/CT and bone scintigraphy for detection of bone metastases in breast cancer. Acta Radiol 2011;52(9):1009–1014.
3. Cook GJ, Houston S, Rubens R, Maisey MN, Fogelman I. Detection of bone metastases in breast cancer by 18FDG PET: differing metabolic activity in osteoblastic and osteolytic lesions. J Clin Oncol 1998;16(10):3375–3379.
4. Ng SH, Chan SC, Yen TC, et al. Staging of untreated nasopharyngeal carcinoma with PET/CT: comparison with conventional imaging work-up. Eur J Nucl Med Mol Imaging 2009;36(1):12–22.
5. Damle NA, Bal C, Bandopadhyaya GP, et al. The role of 18F-fluoride PET-CT in the detection of bone metastases in patients with breast, lung and prostate carcinoma: a comparison with FDG PET/CT and 99mTc-MDP bone scan. Jpn J Radiol 2013;31(4):262–269.
6. Pasoglou V, Michoux N, Peeters F, et al. Whole-body 3D T1-weighted MR imaging in patients with prostate cancer: feasibility and evaluation in screening for metastatic disease. Radiology 2015;275(1):155–166.
7. Groves AM, Beadsmoore CJ, Cheow HK, et al. Can 16-detector multislice CT exclude skeletal lesions during tumour staging? implications for the cancer patient. Eur Radiol 2006;16(5):1066–1073.
8. Kalogeropoulou C, Karachaliou A, Zampakis P. Radiologic evaluation of skeletal metastases: role of plain radiographs and computed tomography. In: Kardamakis D, Vassilious V, eds. Bone metastases. Berlin, Germany: Springer, 2009; 119–136.
9. Ishida T, Ashizawa K, Engelmann R, Katsuragawa S, MacMahon H, Doi K. Application of temporal subtraction for detection of interval changes on chest radiographs: improvement of subtraction images using automated initial image matching. J Digit Imaging 1999;12(2):77–86.
10. Abe H, Ishida T, Shiraishi J, et al. Effect of temporal subtraction images on radiologists' detection of lung cancer on CT: results of the observer performance study with use of film computed tomography images. Acad Radiol 2004;11(12):1337–1343.

11. Aoki T, Murakami S, Kim H, et al. Temporal subtraction method for lung nodule detection on successive thoracic CT soft-copy images. Radiology 2014;271(1):255–261.
12. Beigelman-Aubry C, Raffy P, Yang W, Castellino RA, Grenier PA. Computer-aided detection of solid lung nodules on follow-up MDCT screening: evaluation of detection, tracking, and reading time. AJR Am J Roentgenol 2007;189(4):948–955.
13. Shiraishi J, Appelbaum D, Pu Y, Li Q, Pesce L, Doi K. Usefulness of temporal subtraction images for identification of interval changes in successive whole-body bone scans: JAFROC analysis of radiologists' performance. Acad Radiol 2007;14(8):959–966.
14. Dorfman DD, Berbaum KS, Metz CE. Receiver operating characteristic rating analysis. generalization to the population of readers and patients with the jackknife method. Invest Radiol 1992;27(9):723–731.
15. Chakraborty DP, Berbaum KS. Observer studies involving detection and localization: modeling, analysis, and validation. Med Phys 2004;31(8):2313–2330.
16. Cao K, Ding K, Amelon RE, et al. Intensity-based registration for lung motion estimation. In: Ehrhardt J, Lorenz C, eds. 4D Modeling and estimation of respiratory motion for radiation therapy. Berlin, Germany: Springer, 2013; 125–158.
17. Hodneland E, Hanson EA, Lundervold A, Modersitzki J, Eikefjord E, Munthe-Kaas AZ. Segmentation-driven image registration-application to 4D DCE-MRI recordings of the moving kidneys. IEEE Trans Image Process 2014;23(5):2392–2404.
18. Wu G, Wang Q, Lian J, Shen D. Reconstruction of 4D-CT from a single free-breathing 3D-CT by spatial-temporal image registration. Inf Process Med Imaging 2011;22:686–698.
19. Sakamoto R, Mori S, Miller MI, Okada T, Togashi K. Detection of time-varying structures by large deformation diffeomorphic metric mapping to aid reading of high-resolution CT images of the lung. PLoS One 2014;9(1):e85580.
20. O'Connor SD, Yao J, Summers RM. Lytic metastases in thoracolumbar spine: computer-aided detection at CT—preliminary study. Radiology 2007;242(3):811–816.
21. Burns JE, Yao J, Wiese TS, Muñoz HE, Jones EC, Summers RM. Automated detection of sclerotic metastases in the thoracolumbar spine at CT. Radiology 2013;268(1):69–78.
22. Hammon M, Dankerl P, Tsymbal A, et al. Automatic detection of lytic and blastic thoracolumbar spine metastases on computed tomography. Eur Radiol 2013;23(7):1862–1870.
23. Kakhki VR, Anvari K, Sadeghi R, Mahmoudian AS, Torabian-Kakhki M. Pattern and distribution of bone metastases in common malignant tumors. Nucl Med Rev Cent East Eur 2013;16(2):66–69.